Post-print of International Journal of Hydrogen Energy, Volume 44, Issue 25, 5th January 201

a) Manuscript title

Effect of oxidation-reduction cycles on Steam-Methane reforming kinetics over a nickel-based catalyst

b) Authors reference and address:

M.V. Navarro, J. Plou, J.M. López, G. Grasa, R. Murillo

Department of Energy and Environment, Instituto de Carboquímica (ICB-CSIC), C/ Miguel Luesma Castán 4, 50018 Zaragoza, Spain

Corresponding author: Dr. Maria Victoria Navarro

Department of Energy and Environment, Instituto de Carboquímica (ICB-CSIC), C/Miguel Luesma Castán 4, 50018-Zaragoza, Spain

Phone: +34 976 733977, Fax: +34 976 733318

e-mail: navarro@icb.csic.es

c) Number of pages, tables and figures

This manuscript has 29 pages, 2 Tables and 9 Figures

Effect of oxidation-reduction cycles on Steam-Methane reforming kinetics over a nickel-based catalyst

M.V. Navarro*, J. Plou, J.M. López, G. Grasa, R. Murillo

Department of Energy and Environment, Instituto de Carboquímica (ICB-CSIC),

C/ Miguel Luesma Castán 4, 50018 Zaragoza, Spain

ABSTRACT

The paper presents a detailed analysis of the effect of a high number of oxidation-reduction cycles on the steam-methane reforming process over a commercial Ni-based catalyst under conditions of intrinsic kinetics. These cycles take place within the sorption-enhanced steam-methane reforming process for hydrogen production including sorbent regeneration step. Experiments of steam-methane reforming and reverse water-gas shift reactions were carried out to obtain a complete characterisation of the system kinetics. After 80 cycles, methane conversion increased, while carbon dioxide conversion remained fairly constant. After 125 cycles, methane showed no significant changes in conversion compared to the increase exhibited by carbon dioxide. The kinetic model of Xu and Froment fitted the experimental results to provide the activation energies of the main reactions, which presented an evolution with redox cycles in line with the trends observed for conversion. The reactions with methane initially reduced their activation energy, facilitating conversion, while the reactions with carbon dioxide initially kept the activation energy constant, subsequently reducing it.

Keywords: Hydrogen production; Sorption-enhanced steam-methane reforming; Kinetics; Catalyst; Redox cycles

Corresponding author. Tel: +34 976733977; fax: +34 976733318.

E-mail address: navarro@icb.csic.es (María Victoria Navarro)

1. Introduction

Steam-methane reforming (SMR) is the most commonly used process for hydrogen (H_2) production, although there is a high level of associated carbon dioxide (CO_2) emissions, some 3 kg of CO_2 being produced per kg of methane consumed, without taking into account additional fuel requirements for high process temperature operation [1]. CO_2 is a greenhouse gas and an undesired diluent for more valuable products [2]. The sorption-enhanced steam-methane reforming process (SE-SMR) enhances hydrogen production with in-situ CO_2 capture and significant energy saving potential by process intensification features and milder reactive conditions [3]. The concept behind this process is based on the use of a reforming catalyst in combination with a selective and regenerable solid sorbent to remove CO_2 from the reaction zone. In addition, the removal of one of the products shifts the equilibrium of the reversible SMR and water-gas shift (WGS) reactions, enhancing hydrogen production based on Le Chatelier's principle [4]. However, in practical applications the investigated materials are bound to face alternatively reforming and sorbent regeneration conditions in cyclical performance [2].

Innovative processes [3, 5-9] have proposed the coupling of sorption enhancement and chemical looping together for endothermic reactions like steam reforming. The process first named Unmixed Steam Reforming (USR) was later termed Sorption Enhanced Chemical Looping Reforming (SE-CLSR) [3]. They proposed to use the exothermic oxidation of Ni to provide the amount of heat required for calcination of $CaCO_3$ back to CaO. When the conditions are such that all of the metal is fully oxidized and fully reduced during each cycle, then heat can be uniformly generated throughout the volume of the reactor [6]. Abanades et al. [10] also developed a process that coupled a second Cu/CuO chemical loop to solve the problem of the endothermic $CaCO_3$

52 calcination. The latter process was designed to be carried out in fixed-bed reactors
53 adiabatically operated in parallel at three main reaction stages: i) SE-SMR to produce
54 hydrogen; ii) oxidation to prepare the Cu based material for reduction; and iii)
55 exothermic reduction of CuO to provide the required energy to regenerate the sorbent
56 by calcination. One of the current challenges faced is to find appropriate materials to
57 enable this to be performed adequately in a multi-cyclic oxidation-reduction-reforming
58 operation. With regard to the application of catalysts in this process, it is of great
59 interest to understand the effect of an increasing number of redox cycles on the
60 equilibrium activity and kinetics of the catalyst in the SMR reaction.

61 The reforming step of SE-SMR processes is carried out at remarkably lower
62 temperatures and pressures (700–1000 K and 1–15 bar) [11-25] than those generally
63 applied in SMR processes (typically 1100–1200 K and 15–20 bar) [26]. Under these
64 conditions, catalysts can suffer from carbon formation and oxidation by steam effect
65 [27], formation of spinels [28], agglomeration of Ni crystallites [21] or Ni crystallite
66 growth [15, 20]. Moreover, the periodic change in the catalyst environment produces
67 enlargement and reduction of molar volumes from reduced metallic Ni^0 to oxidised NiO
68 [21, 29]. Many studies on SE-SMR process have applied commercial SMR catalysts.
69 However, the number of studies dealing with catalyst cycling through a high number of
70 reforming/regeneration stages is limited in literature, although catalyst stability is a key
71 parameter for a potential SE-SMR process development. Feng et al. [30] observed an
72 increase in the nickel particle size from 21 to 107.7 nm in 7 temperature cycles from
73 873 K in the step for hydrogen production to 1073 K in the regeneration step. Lysikov
74 et al. [21] studied the evolution of a pristine catalyst consisting of nano-sized nickel
75 oxide particles with an average diameter of 5–10 nm influenced by redox cycling. The
76 authors determined a growth in the active component to 100–200 nm after 100 cycles.

Lopez-Ortiz and Harrison [22] reported a different pattern of Ni crystallite growth due to regeneration stages under inert atmosphere depending on regeneration temperature, 1073 K and 1223 K. For the initial cycles, the active phase presented a similar crystallite size increase at both temperatures, to 25.4 nm and 26.3 nm, respectively. However, an additional increase occurred at 1223 K regeneration, reaching 32.2 nm in the 15^{th} cycle, compared to the crystallite size increase produced with regeneration at 1073 K to 27.2 nm after 25 cycles. Our group [31] evaluated the effect of 200 redox cycles on catalyst performance under SE-SMR conditions. The experimental results obtained with the aged catalyst mixed with fresh sorbent showed that in both pre and post-breakthrough periods, the composition obtained in every experiment closely reproduced the values calculated for thermodynamic equilibrium. Additionally, the same level of reforming activity was found at temperatures between 773 K and 973 K, steam to methane ratio (S/C) of 3 and mass hourly space velocity of methane (CH_4) of 8.8 $kg_{CH4}/h\ kg_{cat}$ for the fresh catalyst and the catalyst cycled 100 times [32]. After 200 redox cycles performed at 1123 K, some deactivation was observed in the reforming activity of the catalyst in line with an increase in the main Ni crystallite size from 9 to 55 nm, although the occurrence of some Ni nanocrystallites of lower size was still observed. The discrepancies between the experimental and theoretical data of equilibrium indicate that there were changes in the catalytic SMR kinetics.

The main chemical reactions that take place in SMR have been identified as follows:

$$CH_4(g) + H_2O(g) \leftrightarrow CO(g) + 3H_2(g) \qquad \Delta H_{298K} = +206.2\ kJ/mol \qquad (R.1)$$

$$CO(g) + H_2O(g) \leftrightarrow CO_2(g) + H_2(g) \qquad \Delta H_{298K} = -41.5\ kJ/mol \qquad (R.2)$$

$$CH_4(g) + 2H_2O(g) \leftrightarrow CO_2(g) + 4H_2(g) \qquad \Delta H_{298K} = +164.9\ kJ/mol \qquad (R.3)$$

101 The overall SMR process is endothermic in nature and requires additional heat
102 to proceed. Catalytic SMR is a complex process involving the diffusion of reactants
103 through bulk gas phases to the surface of the catalyst particles, adsorption and reaction.
104 Many side reactions may also take place [33]. The kinetics of these reactions has been
105 extensively studied, leading to the controversial mechanisms and kinetics SMR found in
106 the literature [34]. Xu and Froment [35] proposed one of the earliest expressions with a
107 detailed mechanism over a $Ni/MgAl_2O_3$ catalyst, with kinetic rate equations based on
108 the Langmuir-Hinshelwood approach with model discrimination and parameter
109 estimation. The model developed by Numaguchi and Kikuchi [36] assumed the
110 competitive production model of CO and CO_2 and only takes into account reactions 1
111 and 2. Hou and Hughes [37] derived intrinsic rate equations by using the Langmuir-
112 Hinselwood-Hougen-Watson approach and Freundlich's adsorption concept. A different
113 approach was proposed by Wei and Iglesia [38], who investigated the mechanism for
114 the reactions of CH_4 with CO_2 and H_2O on different metal clusters. They concluded that
115 the reactivity of the metal towards C–H bond breaking governs the overall reaction
116 kinetics.
117 The aim of the present research was to analyse and evaluate the performance of
118 a commercial Ni-based reforming catalyst under conditions in the region of the intrinsic
119 kinetics of SMR coupled with redox stages that have not been reported yet. The model
120 developed by Xu and Froment [35], which has demonstrated to be more general than
121 other models [33], was used to fit new kinetic constants for this catalyst into two
122 different sets of reactions, SMR and reverse water-gas shift (RWGS). Two more sets of
123 experiments were performed after 80 and 125 redox cycles to evaluate the changes in
124 catalyst performance and fit the corresponding kinetic constants. For the first time in the

literature, to our knowledge, the kinetic parameters obtained for the fresh catalyst were compared with the parameters calculated for a highly cycled catalyst in redox stages.

2. Experimental and kinetic model

A commercial reforming catalyst, HiFUEL® R110, was supplied by Johnson Matthey in 4-hole quadralobe pellet form. The content of Ni active phase supported on $CaAl_2O_4$ was determined by element analysis as 15.9–20.0 wt% [32]. This solid was crushed and sieved to a particle size ~~of~~ between 100 μm and 200 μm for the experiments.

The main properties of fresh and reduced catalyst were previously analysed [32] through different characterisation techniques. Powder X-Ray diffraction spectroscopy (XRD) was utilised to identify the crystalline phases present in the fresh sample. A Bruker D8 Advance diffractometer with monochromatic Cu Kα source, operated at 40 kV and 40 mA, was used. The experimental patterns were calibrated against a silicon standard and the crystalline phases were identified by matching the experimental patterns to the JCPDS powder diffraction file database. Scanning electron microscopy (SEM) was also applied to the fresh sample to determine the nickel distribution on the support. A Hitachi S-3400 N model coupled to Röntec XFlash EDX was used.

SMR experiments were carried out with 0.005 g of catalyst mixed with SiC provided by VWR Chemicals BDH Prolabo (201 μm average particle size) introduced to prevent problems of dispersion and to reduce temperature changes. The sample was placed in an atmospheric system, described previously [31], with a tubular quartz reactor of 300 mm of length, an inner diameter of 6.8 mm and a total bed length range of 10 mm. The reactor was located inside a cylindrical electrically heated oven controlled by a PID controller and a thermocouple placed in the middle of the sample.

150 The gas mixture was prepared by a set of mass flow controllers calibrated for CH_4, CO_2,
151 H_2, O_2, Ar and water. For the SMR tests, the water flow was mixed with CH_4 and H_2
152 and evaporated in a stainless steel pipe heated to 673 K by a cylindrical electric furnace
153 connected to a temperature controller. The different feed mixtures were stabilised in a
154 secondary line before passing through the reactor where the catalyst was placed. A
155 pressure gauge located before the reactor measured the reaction pressure. A recovery
156 system to condense water was positioned after the reactor. Finally, aliquots of the outlet
157 gas stream were analysed online using a quadrupole spectrometer (Omnistar, Pfeiffer
158 Vacuum). The following masses were monitored: m/z =2 for H_2, m/z =15 for CH_4,
159 m/z=18 for water, m/z = 28 for CO, m/z=32 for O_2 m/z = 40 for Ar and both m/z= 28
160 and 44 for CO_2.

161 The routine for the tests in the experimental facility was as follows: before each
162 reforming test, the catalyst was heated in Ar atmosphere and, then, reduced in situ for
163 30 min at 1123 K with 10 % H_2 balance in Ar (total flow of 33.3 mlN/min). The
164 catalytic activity of the sample was subsequently measured at temperatures limited to
165 values that avoided measuring only equilibrium conversion [35] at 748 K, 773 K, 798
166 K, 823 K and 848 K for 30 min each. The S/C ratio used was 3, and hydrogen was
167 added to the reactant feed in the hydrogen-to-methane ratio (H_2/CH_4) of 1 to avoid
168 reoxidation of the catalyst by steam [35]. The sample was then oxidised for 30 min at
169 1123 K with 10 vol% O_2 balance in Ar (total flow of 33.3 mlN/min) and reduced at the
170 described reduction conditions. The reforming activity of the catalyst was tested again,
171 changing space-time from 0.12 to 0.19, 0.25 and 0.37 $g_{cat}{\cdot}h/mol_{CH4}$. Catalyst activity
172 was measured with the same procedure in the RWGS and methanation reactions.
173 Catalytic activity in these reactions was measured at 598 K, 623 K, 648 K and 673 K for
174 30 min each at space-times of 0.21, 0.25 and 0.3 $g_{cat}{\cdot}h/mol_{CO2}$ with a hydrogen-to-

carbon dioxide (H_2/CO_2) ratio of 0.75. These experimental conditions were specially chosen to assure intrinsic kinetic control and closely reproduce the conditions used by Xu and Froment [35] to develop the kinetic model. To increase the number of cycles followed by the catalyst, successive oxidation and reduction reactions were carried out at 1123 K under 10 vol% O_2 (balanced by Ar) and 10 vol% H_2 (balanced by Ar), respectively. All the experiments were performed with one load of catalyst, for the purpose of ageing the catalyst at the same time as determining the kinetics, since the study was focused on the effect of short redox and reforming stages on the catalyst performance. Catalyst activity was then restored by the hydrogen re-reduction step.

The conversion of CH_4 and its conversion into CO_2 were calculated from the effluent concentrations via [40, 41]:

——————————— (1) ——————————— (2)

Likewise, the conversion of CO_2 and its conversion into CH_4 were calculated with the following equations:

——————————— (3) ——————————— (4)

Xu and Froment [35] developed one of the best-known SMR kinetic models on the basis of the three equilibrium reactions, R.1–3 described above. It was considered helpful to introduce experimental results from RWGS tests at lower temperatures in order to obtain more accurate value estimations for the kinetic parameters [36]. Thus, the kinetic expressions used are:

—— ——————————— (5)

—— ——————————— (6)

—— ——————————— (7)

198 (8)

199 where p_i is the partial pressure of every component (bar). k_1 (kmol·bar$^{0.5}$/kg$_{cat}$·h),
200 k_2 (kmol/kg$_{cat}$·h·bar) and k_3 (kmol·bar$^{0.5}$/kg$_{cat}$·h) are the rate coefficients and K_1 (bar^2),
201 K_2 (-), K_3 (bar^2) are the equilibrium constants of reactions R.1–3, respectively. Finally,
202 K_{CH4} (1/bar), K_{CO} (1/bar) and K_{H2} (1/bar) are the adsorption constants of these
203 compounds, and K_{H2O} (-) is the dissociative adsorption constant of H_2O.

204 The reaction rates for disappearance of reactants and formation of products are
205 obtained from the following equations 5 to 8 while the reaction rates for H_2, H_2O and
206 CO are predicted from the stoichiometric coefficients of every component in reactions
207 R.1–3.

208 (9) (11)

209 (10) (12)

210 The model is a Langmuir-Hinshelwood model accounting for the adsorption of
211 CO, and H_2 on the same site occupied by CH_4 and H_2O, thus, the reactions between
212 adsorbed species are assumed to be the rate determining the steps [27]. Accordingly, the
213 study focused on the estimation of the rate coefficients at different temperatures and the
214 evolution with redox cycles of the activation energies and pre-exponential factors of the
215 reactions R. 1–3. All the parameters calculated to apply the model at the test
216 temperatures are compiled in Table 1.

217 The dependence of the rate coefficients (k_1, k_2, k_3) with temperature was
218 described by an Arrhenius type function:

219 (13)

220 where k_{0i} and E_i (kJ/mol) are the pre-exponential factors and activation energy
221 for each reaction. T is temperature (K) and R is the ideal gas constant (kJ/mol·K)

222

223 **Table 1.** Parameters used in the kinetics estimation.

T (K)	*K_{1eq} (bar^2)	*K_{2eq}	*K_{3eq} (bar^2)	**K_{CH4}	**K_{H2O}	**K_{H2}	**K_{CO}
Steam Methane Reforming							
748	0.0030	6.11	0.0185	0.3137	0.1132		
773	0.0095	5.03	0.0480	0.2570	0.1795		
798	0.0281	4.20	0.1180	0.2133	0.2766		
823	0.0776	3.55	0.2755	0.1790	0.4152		
848	0.2024	3.03	0.6136	0.1518	0.6084		
Reverse Water-Gas Shift							
598	$4.43 \cdot 10^{-7}$	28.63	$1.27 \cdot 10^{-5}$			0.1072	122.47
623	$2.56 \cdot 10^{-6}$	20.92	$5.36 \cdot 10^{-5}$			0.0549	69.24
648	$1.30 \cdot 10^{-5}$	15.69	$2.04 \cdot 10^{-4}$			0.0296	40.91
673	$5.87 \cdot 10^{-5}$	12.05	$7.07 \cdot 10^{-4}$			0.0167	25.13

224 *Values calculated with HSC Chemistry Software.
225 **Values calculated with expressions provided by [35].
226

227 # 3. Results and discussion

228 ## 3.1. Physicochemical properties of fresh materials

229 Textural characterisation was performed on the fresh material [32] to obtain the
230 values of helium density, 3.4 g/cm^3; mercury porosity, 0.41; BET surface area, 25 m^2/g;
231 and mean pore size, 14 nm. The two latter values were calculated from the N_2 isotherm.
232 These values are in the range of data previously presented in the literature [42–44]. H_2
233 consumption, calculated from successive TPR/TPO cycles [32], which mimic the first
234 steps of the cyclic process studied in this work, decreased from 67.2 cm^3/g in the first
235 cycle to a fairly constant value of 61.1 cm^3/g. However, from the H_2 consumption
236 profiles obtained, a shift was observed in the main consumption temperatures from
237 higher (600 K to 1100 K) to lower temperatures (500 K to 900 K). This change was
238 attributed [32] to the transformation of prevalent amorphous Ni-Ca-Al species into NiO
239 species with weaker interaction with the support, facilitating material reducibility.

240 Figure 1 shows the XRD pattern of the fresh and reduced catalyst, where the
241 characteristic peaks of NiO and metallic Ni can be observed for the fresh and reduced
242 sample, respectively. Al_2O_3 and $CaO(Al_2O_3)_2$ phases are also distinguished for both

243 samples. From this pattern, the initial Ni crystallite size was calculated by the Rietveld
244 method as 9 nm.

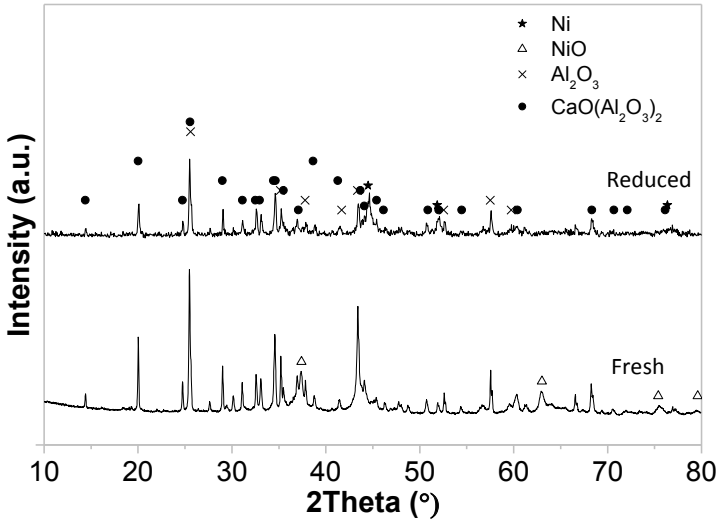

245

246 **Fig. 1.** XRD patterns of fresh and reduced Ni catalyst.
247
248 The SEM analyses of the reduced catalyst, compiled in Figure 2, show similar
249 images of the fresh and reduced Ni catalyst with an initial good Ni distribution (small
250 white spots identified by EDX) all over the support surface.

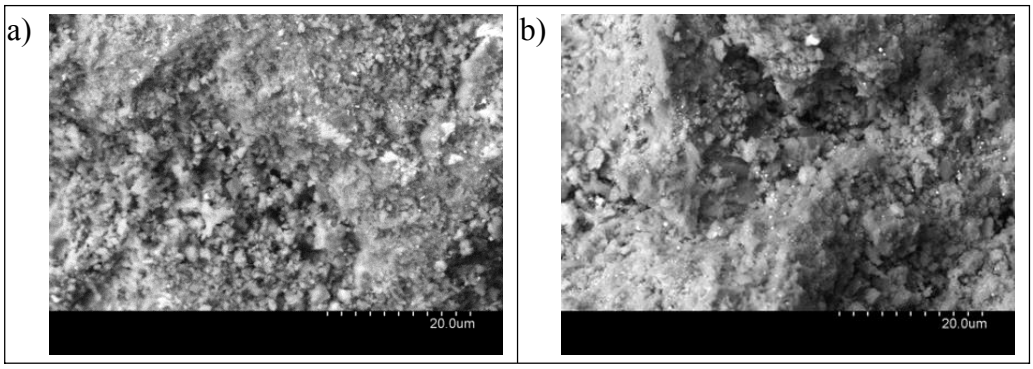

251
252 **Fig. 2. SEM** images of a) fresh sample and b) reduced sample

253

254 **4.2. Steam-Methane Reforming. Effect of temperature and space-time on methane**
255 **conversion**

256 The thermodynamic relationships for SMR limit any kinetic study to a rather
257 narrow temperature range. Also reaction pressure and total flow rate are limited by the

equipment [37]. The experimental conditions used in this work for the generation of conversion results, four space-times at five different temperatures, are described in the experimental section.

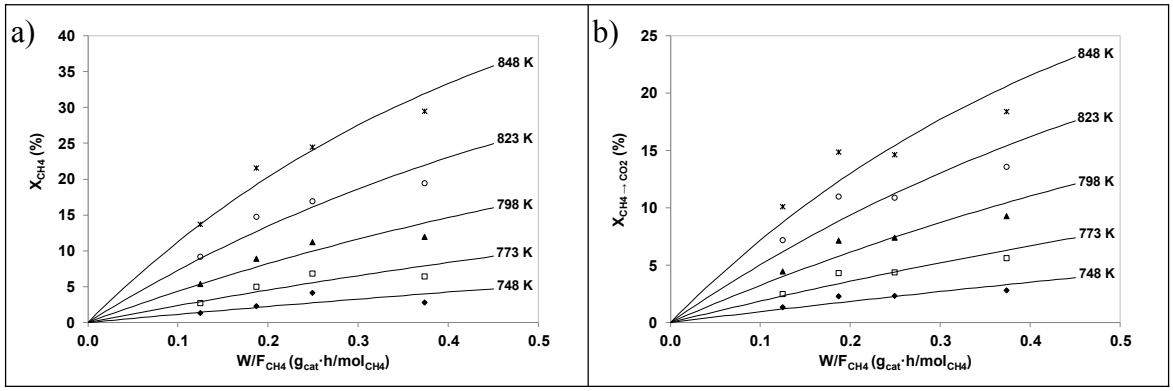

Fig. 3. Conversion of CH_4 vs space-time . a) total CH_4 conversion, b) conversion of CH_4 into CO_2. Dots: experimental values, lines: exponential regression lines. P = 1 bar, S/C = 3, H_2/CH_4 = 1.

Figure 3 shows the curves obtained for total CH_4 conversion and the conversion of CH_4 into CO_2 vs space-time. The typical experimental data of total CH_4 conversion vs are compiled in Figure 3.a. These tests were performed at low temperatures to avoid measuring only equilibrium conversions. As expected for an endothermic process, a positive effect of temperature can be observed in these figures for both total conversion and the conversion of CH_4 into CO_2. It was also observed that conversion increased with increasing space-time resulting from an increase in contact time between reactants and catalyst. Many reactions are involved in SMR, and the conditions used greatly affect product composition. In Figure 3.b, the conversion of CH_4 into CO_2 at different temperatures is compiled vs space-time. The high conversion into CO_2 at low CH_4 conversions suggests that the main primary product is CO_2, as previously observed by other authors [37]. However, this also means that carbon monoxide is present as a product of the reaction at higher temperatures. Overall carbon balances with CH_4, CO_2

and CO were better than 95 % for all the experiments performed within the same range as found in previous publications [37].

3.3. Reverse Water-Gas Shift. Effect of temperature and space-time on carbon dioxide conversion

As the WGS reaction was essentially at thermodynamic equilibrium during SMR at the temperatures tested from 748 K to 848 K, it was considered helpful to carry out the RWGS reaction at lower temperatures in order to obtain more accurate estimates for the kinetic parameters [36]. Three different space-times at four different temperatures were studied with an H_2/CO_2 ratio of 0.75 in feed composition. As in SRM, temperature presents a positive effect on both the conversion of CO_2 and its conversion into CH_4. The increase in CO_2 conversion with space-time for different temperatures is shown in Figure 4.a. Conversion of CO_2 into CH_4 is equally shown in figure 4.b where a monotonic increase with space-time is observed. This CH_4 could be generated directly by methanation of CO_2 or indirectly through the CO also present in the gas product stream, which makes the conversion into CH_4 three or four times lower than the total CO_2 conversion. At the applied conditions, the progress of both reactions was low, producing low CO_2 conversion values up to 12 % and conversion into CH_4 lower than 3 %.

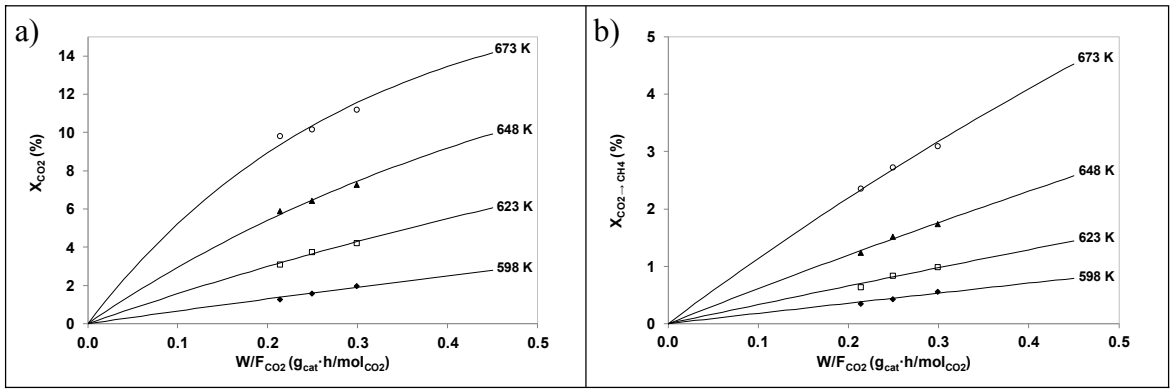

Fig. 4. CO_2 conversion vs space-time . a) total conversion of CO_2, b) conversion of CO_2 into CH_4. Dots: experimental values, lines: exponential regression lines. P = 1 bar, H_2/CO_2 = 0.75

3.4. Effect of redox cycles on catalyst performance

As previously explained, SE-SMR processes require the addition of a regeneration stage of calcination with high energy demand. Some innovative processes propose that part of the required energy should be obtained from loops of Ni/NiO [5-9] or Cu/CuO [10], with sequential changing of conditions. The changes in the molar volumes associated with the oxidation of Ni to NiO and subsequent reduction to Ni could affect catalyst performance [21, 29]. In order to determine the cyclic behaviour of the catalyst, the fresh catalyst sample was first aged through a total of 80 ~~redox~~ cycles of oxidation and reduction reactions at conditions described in the experimental section before studying the reforming and RWGS reactions again. The sample was then aged through a total of 125 redox cycles to once again study the reforming and RWGS reactions. Figure 5 shows the activity of the fresh and aged catalyst vs temperature for the SMR and RWGS reactions at the highest space-time studied for each reaction, 0.37 g_{cat}·h/mol_{CH4} and 0.3 g_{cat}·h/mol_{CO2}, respectively. The theoretical equilibrium values are also compiled for comparison.

All the conversion results compiled in Figure 5 were lower than the theoretical equilibrium values (continuous lines in Figure 5) for the entire range of temperatures

322 evaluated. Thus, the experiments were performed under conditions away from the
323 equilibrium. After 80 redox cycles, an increase in total CH_4 conversion and conversion
324 of CH_4 into CO_2 was observed. This increase in catalytic activity could be related to a
325 facilitated reducibility of the active metal on the support surface within increasing
326 number of redox cycles. Experimental results previously obtained for H_2 consumption
327 after ten consecutive TPR/TPO redox cycles [32], showed a change in the TPR profiles
328 obtained with an almost constant total H_2 consumption of 61,1 cm^3/g. Thus, the profiles
329 showed a shift in H_2 consumption with three initial peaks placed from 600 K to 1100 K
330 towards a wider distribution of H_2 consumption at lower temperatures from 500 K to
331 900 K. This fact indicates a redistribution of the Ni species, the prevalent amorphous
332 Ni-Ca-Al species that reduce at high temperatures are transformed into NiO species that
333 reduce at lower temperatures, with a weaker interaction with the support. This weaker
334 interaction between the active phase and the support improves material reducibility that
335 could then facilitate CH_4 conversion. However, total CO_2 conversion sustained the
336 values obtained by the fresh catalyst with a low increase in the conversion of CO_2 into
337 CH_4.
338
339
340
341
342

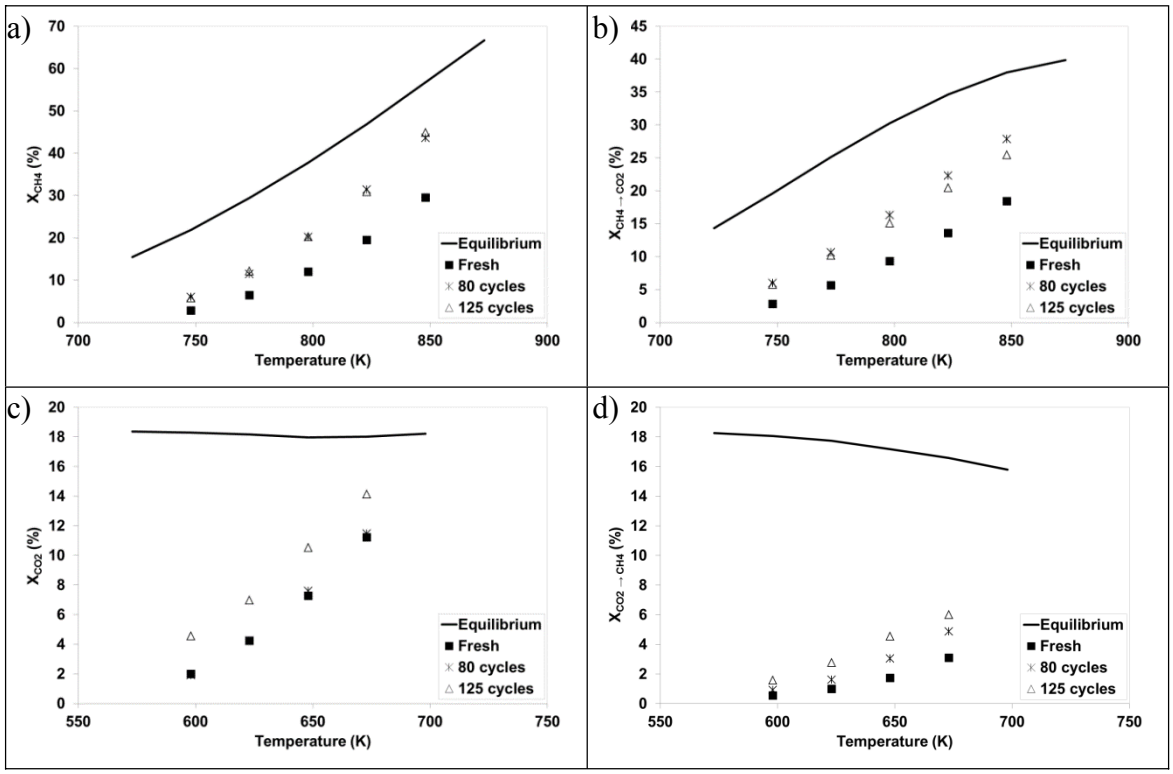

Fig 5. Activity of catalyst vs Temperature after redox cycles. a) total CH_4 conversion, b) conversion of CH_4 into CO_2, c) total CO_2 conversion, d) conversion of CO_2 into CH_4 vs Temperature. Dots: experimental values, lines: equilibrium values. SMR test conditions: P = 1 bar, S/C = 3, H_2/CH_4 = 1, = 0.37 g_{cat}·h/mol_{CH4}. RWGS test conditions: P = 1 bar, H_2/CO_2 = 0.75, = 0.30 g_{cat}·h/mol_{CO2}.

With regard to the main reactions taking place in this process, R.1–3, these results support higher catalyst activity in CH_4 reforming reactions while catalyst activity in the WGS reaction remains constant. With regard to the results obtained after 125 redox cycles, total CH_4 conversion and conversion of CH_4 into CO_2, the values obtained after 80 redox cycles were retained. In these tests a high increase in CO_2 conversion was observed, compared to values obtained in previously performed tests, while CO_2 conversion into CH_4 sustained a monotonically low increase. Based on these results, catalyst activity is mainly kept constant for reactions with CH_4 as a reactant, while it increases for reactions with CO_2 as a reactant.

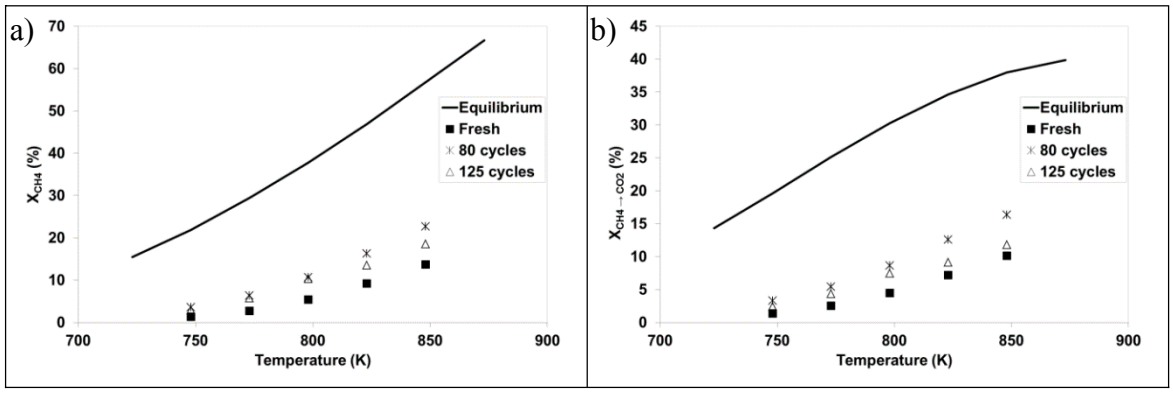

Fig 6. a) Total CH_4 conversion and b) conversion of CH_4 into CO_2 vs Temperature. Dots: experimental values, line: equilibrium values. SMR test conditions: P = 1 bar, S/C = 3, H_2/CH_4 = 1, = 0.12 $g_{cat}\cdot h/mol_{CH4}$.

The previous remarks made from the analysis performed on the results obtained at the highest space-time studied were also made at the other studied space-times – 0.25, 0.19 and 0.12 $g_{cat}\cdot h/mol_{CH4}$ for SRM tests, and 0.25 and 0.21 $g_{cat}\cdot h/mol_{CO2}$ for RWGS tests. All the experiments produced reactant conversions lower than the theoretical equilibrium values, and these reactant conversions retain the same main patterns. On one hand, CH_4 conversion increased with the increasing number of redox cycles up to 80 cycles, to later remain constant after 125 cycles. However, CO_2 conversion was constant for the first cycles, but there was an increase when the catalyst was analysed after 125 redox stages. Nonetheless, a light dependency on temperature could be observed at the lowest studied space-time of 0.12 $g_{cat}\cdot h/mol_{CH4}$, the results of which for the SMR process are compiled in Figure 6. Under the given conditions, catalyst activity after 125 redox cycles at temperatures higher than 800 K was lower than that obtained after 80 cycles. In Figure 6.a a conversion of 23 % was achieved at 850 K after 80 cycles, later decreasing to 19 % after 125 redox cycles. Figure 5.a shows the results obtained at 0.37 $g_{cat}\cdot h/mol_{CH4}$, at which CH_4 conversion of 45 % was observed at 850 K after 80 and 125 redox cycles. A similar trend was observed for the conversion of CH_4 into CO_2, showing that the increase in the space-time had a positive effect on CH_4 conversion at high temperatures.

382

383 **3.5. Steam-Methane Reforming kinetics of fresh and cycled catalyst**

384 Exponential regression was used to correlate the relationships between CH_4
385 conversion and the conversion of CH_4 into CO_2 with space-time. Exponential regression
386 was also used to correlate CO_2 conversion and the conversion of CO_2 into CH_4 with
387 space-time. The relationship for the experiments at a fixed pressure, S/C ratio and
388 H_2/CO_2 ratio was obtained as follows:

389 (14)

390 By differentiating this equation, the reactant disappearance rate and product
391 formation rate can be given as:

392 ——— (15)

393 In these equations X_A is the total conversion of reactants X_{CH4}, X_{CO2} or the
394 conversion of reactants to these compounds as products $X_{CH4\rightarrow CO2}$, $X_{CO2\rightarrow CH4}$. The
395 factor X_{eq} is equal to the equilibrium conversion calculated by HSC software at the
396 studied temperatures for reactants X_{CH4eq}, X_{CO2eq} and the conversion of reactants to the
397 products, $X_{(CH4\rightarrow CO2)eq}$, $X_{(CO2\rightarrow CH4)eq}$, depending on the set of experimental data fitted.
398 The parameters B and n were fitted for every set of data points at the same temperature,
399 with the sum of squared errors (SSE) minimised using the GRG non-linear solver in
400 Microsoft Excel.

401 To estimate the kinetic parameters, a method based on the minimisation of SSE
402 was applied to the experimental and predicted reaction rates. The experimental reaction
403 rates were obtained from Eq. 15 applied to SMR and RWGS reactions and the actual
404 compounds. The predicted reaction rates were calculated with Eqs 5–12 using the
405 equilibrium and adsorption parameters compiled in Table 1.

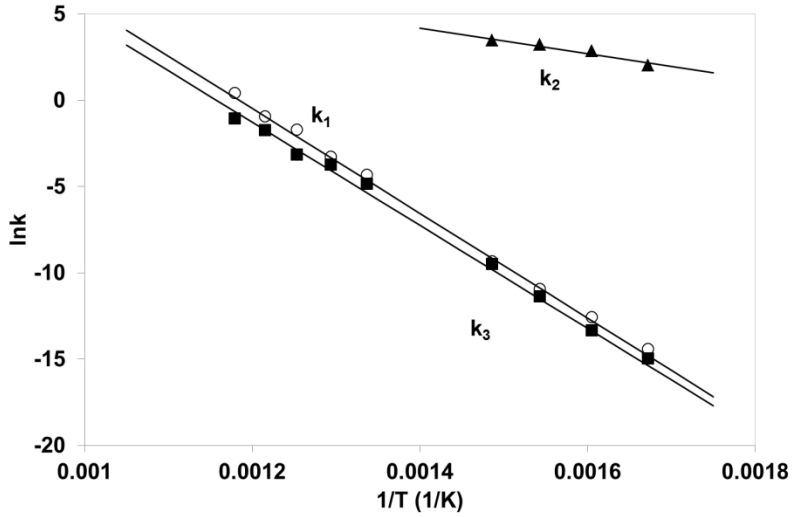

Fig. 7. Temperature dependence of rate constants for fresh catalyst.

After successive iterations, the estimated values of every rate constant were obtained and all of them were related to the temperature dependency on the linearized expression of the Arrhenius Eq. 13. The results obtained with the fresh catalyst are shown in Figure 7. The slope of the lines in Figure 7 gave the value of the activation energies, while the y-intercept provided the value of pre-exponential factors of the kinetic constants [33]. The same procedure was applied to the results obtained for the cycled catalyst. The values for the activation energies and pre-exponential factors obtained for the fresh and cycled catalyst are listed in Table 2 and compared to the values published by Xu and Froment [35].

Table 2. Pre-exponential factors and activation energies for the SMR process via reactions R.1–3.

	Xu and Froment [35]	**Fresh**	**80 cycles**	**125 cycles**
$\mathbf{k_{01}}$	$4.225 \cdot 10^{15}$	$3.95 \cdot 10^{15}$	$4.66 \cdot 10^{15}$	$4.30 \cdot 10^{15}$
$\mathbf{E_1}$ **(kJ/mol)**	240.1	252.2	247.3	244.9
$\mathbf{k_{02}}$	$1.96 \cdot 10^{6}$	$1.98 \cdot 10^{6}$	$2.01 \cdot 10^{6}$	$1.97 \cdot 10^{6}$
$\mathbf{E_2}$ **(kJ/mol)**	67.13	61.3	61.5	55.9
$\mathbf{k_{03}}$	$1.02 \cdot 10^{15}$	$1.01 \cdot 10^{15}$	$8.41 \cdot 10^{14}$	$5.82 \cdot 10^{14}$
$\mathbf{E_3}$ **(kJ/mol)**	243.9	248.2	242.1	247.5

All the calculated activation energies were high, meaning that the rate coefficients satisfied the Arrhenius equations [33]. From the comparison of the fresh

423 catalyst tested in this work with the one tested by Xu and Froment [35], our catalyst
424 presented similar kinetic parameters. The pre-exponential factors were in the same order
425 of magnitude and the activation energies for methane reforming were higher, while
426 those found for WGS were lower than the results obtained by Xu and Froment. The
427 catalysts used for both studies were different – the catalyst used in that work was 15.2
428 wt% Ni supported on $MgAl_2O_3$, while our catalyst was 15.9–20 wt% Ni supported on
429 $CaAl_2O_4$ – and the structural characteristics of active metal nanoparticles and the metal-
430 support interactions strongly affected catalyst activity and furthered its stability or coke
431 resistance [27]. With regard to the activation energies calculated after redox cycling,
432 different trends were observed depending on the presence of CH_4 in the reaction. For
433 reactions R.1 and R.3, the activation energies decreased after the first 80 cycles and also
434 after 125 cycles for R.1. The highest reduction took place after 80 cycles for reaction
435 R.3. For the WGS reaction, the activation energy remained mostly constant after the
436 first 80 redox cycles, greatly decreasing after 125 cycles.
437

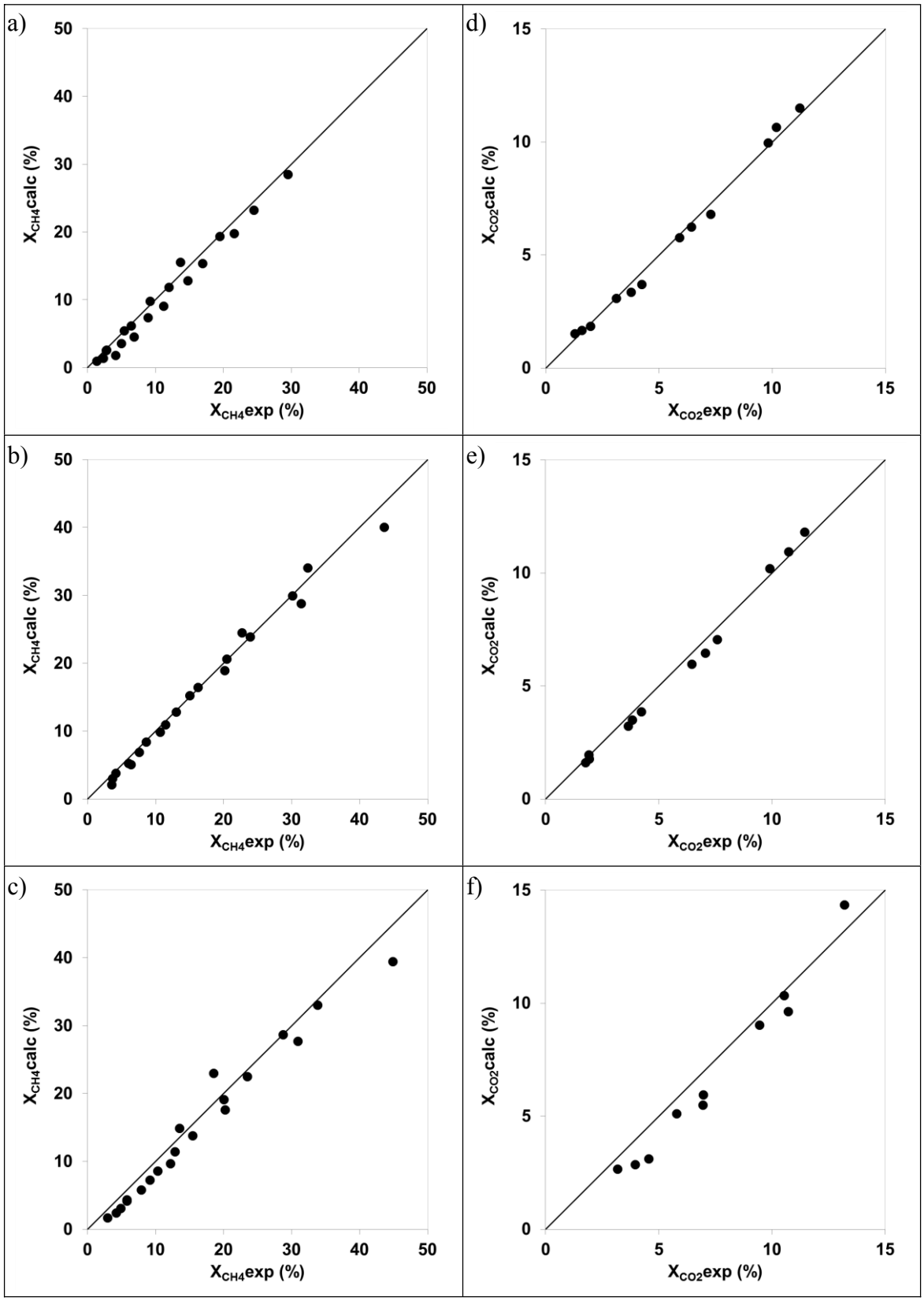

Fig 8. Comparison of experimental and calculated total conversion of CH_4 (a, b, c) and CO_2 (d, e, f) with fresh catalyst, after 80 redox cycles and 125 redox cycles.

442 The evolution of activation energies observed for the three reactions were in line
443 with the trends observed previously for CH_4 and CO_2 conversion in Figure 5, since there
444 was an inverse relationship between activation energy and catalyst activity [20, 27].
445 CH_4 conversion increased after 80 redox cycles, supported by a decrease in the
446 activation energy of reactions R.1 and R.3, although both CH_4 conversion and activation
447 energies remained mostly constant after 125 cycles. However, CO_2 conversion after 80
448 cycles remained the same, as well as the activation energy of reaction R.2, whereas CO_2
449 conversion decreased after 125 cycles, with an increase in the activation energy that
450 reduced the activity of the sample.
451 Figure 8 provides a comparison of the experimental total conversion of CH_4 and
452 CO_2 vs the calculated data with the fitted kinetic parameters of pre-exponential factors
453 and activation energies included in Table 2 for the fresh and cycled catalysts. It can be
454 seen in this figure that the deviation is small, indicating the good consistency of the
455 kinetic parameters. It shows that the model predictions slightly underestimated CH_4
456 conversion, mainly in the lower range. This trend was observed for both SMR and
457 RGWS tests, and also with the fresh sample and after redox cycling. In the case of
458 RGWS tests, CO_2 conversion was directly related to temperature, thus the model
459 slightly underestimated conversion at low temperatures and overestimated it at the
460 highest temperature studied. This trend was more evident in the sample cycled 125
461 times.
462

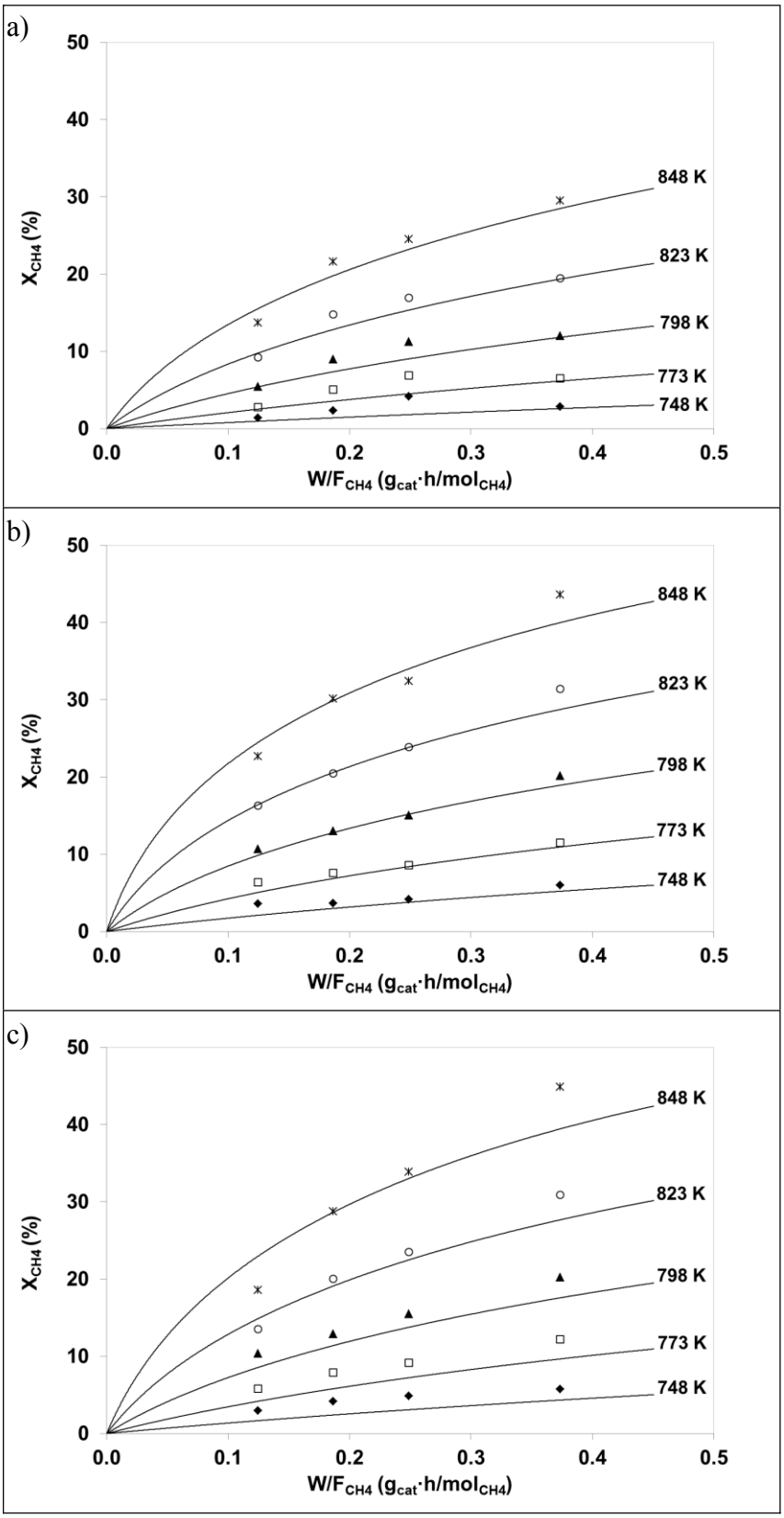

Fig 9. Total CH_4 conversion vs space-time . a) fresh catalyst, b) after 80 redox cycles, c) after 125 redox cycles. Dots: experimental values, lines: fitted values with eqs 1–10 and values from Table 1. Conditions of SMR tests: P = 1 bar, S/C = 3, H_2/CH_4 = 1

The fit of the experimental data obtained for SRM tests of total CH_4 conversion depending on the space-time and temperature can be seen from the comparison with calculated results in Figure 9, for fresh and aged catalyst. It can be observed that the set of data used with the fitted values on Table 2 produce a very good estimation of the experimental conversion results. The fitting of the model reproduces both effects of increasing temperature and space-time on increasing CH_4 conversion. Nevertheless, some of these are slight differences for the aged catalyst depending on the space-time studied. On the one hand, the model underestimated the conversion at the highest space-time studied for catalyst performance after 80 and 125 redox cycles. On the other hand, the model overestimated the CH_4 conversion obtained after 125 cycles at the lowest space-time and highest temperatures studied. At these extreme conditions of the study, the possible changes produced in the surface catalyst could have affected not only the chemical reaction kinetics, but also the adsorption kinetics that were not in the scope of this study. Based on these results, further work should be carried out to determinate the influence of an increasing number of cycles on adsorption parameters.

4. Conclusions

The SMR activity of a commercial Ni-based catalyst was studied in the region of intrinsic kinetics under conditions of cyclic SE-SMR coupled to oxidation-reduction stages. The effect of redox cycles on the reforming activity and kinetic parameters of the catalyst was studied after 80 and 125 cycles. The evolution of CH_4 conversion followed an increase in the values obtained from the fresh sample to the sample cycled 80 times, then stabilising to 125 cycles. The trend observed for the conversion of CH_4 into CO_2 was the same, while there was a change in the case of CO_2 conversion. For the fresh catalyst and the catalyst cycled 80 times, the catalyst activity was similar and

493 produced similar total CO_2 conversion values. After 125 redox cycles, the catalyst
494 showed an increase in activity for the RWGS reaction. The kinetic model proposed by
495 Xu and Froment [35] properly fitted the experimental results for sets of SMR and
496 RWGS reactions to the obtained activation energies of the three main reactions
497 involved. The values obtained, which were close to the values calculated by Xu and
498 Froment [35] for a fresh catalyst, presented an evolution with redox cycles in line with
499 the trends observed for conversion of CH_4 and CO_2. For CH_4, the activation energies of
500 R.1 and R.3 decreased first, which enabled an increase in conversion to later stabilize
501 both activation energy and conversion. For CO_2, stability of conversion is observed in
502 the first 80 cycles, followed by an increase in conversion and a related decrease in the
503 activation energy of the RWGS reaction.
504

505 ## Acknowledgements

506 The authors acknowledge support from the European Union Seventh Framework
507 Programme FP7 under grant agreement No. 608512 (ASCENT Project) and the
508 Regional Aragon Government (DGA) under the research groups support programme.
509 The authors wish to thank Johnson Matthey for providing the catalyst sample.
510

REFERENCES

[1] Felice L, Courson C, Foscolo PU, Kiennemann A. Iron and nickel doped alkaline-earth catalysts for biomass gasification with simultaneous tar reformation and CO2 capture, Int Journal Hydrogen Energy 2011;36:5296-310.

[2] Giuliano A, Giancaterino F, Gallucci K, Foscolo PU, Courson C. Catalytic and sorbent materials based on mayenite for sorption enhanced steam methane reforming with different packed-bed configurations Int J Hydrogen Energy 2018;43:21279-80.

[3] Adiya ZISG, Dupont V, Mahmud T. Chemical equilibrium analysis of hydrogen production from shale gas using sorption enhanced chemical looping steam reforming. Fuel Process Technol 2017;159:128-44.

[4] Harrison D. Sorption-Enhanced Hydrogen Production: A Review. Ind Eng Chem Res 2008;47:6486–501.

[5] Kumar R.V., Lyon R.K., Cole J.A. Unmixed Reforming: A Novel Autothermal Cyclic Steam Reforming Process. In: Grégoire Padró C.E., Lau F. (eds) Advances in Hydrogen Energy (2002). Springer, Boston, MA.

[6] Lyon RK, Cole JA. Unmixed combustion: an alternative to fire. Combust Flame 2000;121:249–61.

[7] Dupont V, Ross AB, Hanley I, Twigg MV. Unmixed steam reforming of methane and sunflower oil: A single-reactor process for H_2-rich gas. Int. J. hydro Energy 2007;32:67-79.

[8] Ryden M, Ramos P. H_2 production with CO_2 capture by sorption enhanced chemical-looping reforming using NiO as oxygen carrier and CaO as CO_2 sorbent. Fuel Process Technol 2012;96:27-36.

[9] Antzara A, Heracleous E, Bukur DB, Lemonidou AA. Thermodynamic analysis of hydrogen production via chemical looping steam methane reforming coupled with in situ CO_2 capture. Int J Greenhouse Gas Control 2015;32:115-28.

[10] Abanades JC, Murillo R, Fernandez JR, Grasa G, Martínez I. New CO_2 Capture Process for Hydrogen Production Combining Ca and Cu Chemical Loops. Environ Sci Technol 2010;44:6901-6904.

[11] Hufton JR, Mayorga S, Sircar S_{τ}. Sorption-Enhanced Reaction Process for Hydrogen production. AIChE J 1999;45:248-56.

[12] Johnsen K, Ryu HJ, Grace JR, Lim CJ. Sorption-enhanced steam reforming of methane on a fluidized bed reactor with dolomite as CO_2-acceptor. Chem Eng Sci 2006;61:1195-202.

[13] Lee DK, back IH, Yoon WL. Modeling and simulation for the methane steam reforming enhanced by in situ CO_2 removal utilizing the CaO carbonation for H_2 production. Chem Eng Sci 2004;59:931-42.

[14] Yi KB,. Harrison DP. Low-pressure sorption-enhanced hydrogen production. Ind Eng Chem Res, 2005;44:1665-69.

[15] Essaki K, Muramatsu T, Kato M,. Effect of equilibrium shift by using lithium silicate pellets in methane steam reforming. Int J Hydrogen Energy 2008;33:4555-59.

[16] Balasubramanian B, Lopez-Ortiz A, Kaytakoglu S, Harrison DP.; Hydrogen from methane in a single-step process. Chem Eng Sci 1999;54:3543-52.

[17] Beaver MG, Caram HS, Sircar S. Sorption enhanced reaction process for direct production of fuel-cell grade hydrogen by low temperature catalytic steam-methane reforming. J Power Sources, 2010;195:1998-2002.

[18] Ding Y, Alpay E. Adsorption-enhanced steam-methane reforming. Chem Eng Sci 2000;55:3929-40.

[19] Lee CH, Mun S, Lee KB. Application of multisection packing concept to sorption-enhanced steam methane reforming reaction for high-purity hydrogen production. J Power Sources 2015;281:158-163.

[20] Oliveira ELG, Grande CA, Rodrigues AE. Steam methane reforming in a Ni/Al_2O_3 catalyst: kinetics and diffusional limitations in extrudates. Can J Chem Eng 2009;87:945-56.

[21] Lysikov A, Okunev A, Netskina O. Study of a nickel catalyst under conditions of the SER process: Influence of RedOx cycling. Int J Hydrogen Energy 2013;38:10354-63.

[22] Lopez-Ortiz A, Harrison DP.; Hydrogen production using sorption-enhanced reaction. Ind Eng Chem Res 2001;40:5102-09.

[23] Li ZS, Cai NS, Yang JB. Continuous production of hydrogen from sorption-enhanced steam methane reforming in two parallel fixed-bed reactors operated in cyclic manner. Ind Eng Chem Res 2006;45:8788-93.

[24] Martavaltzi CS, Pampaka EP, Korkakaki ES, Lemonidou AA. Hydrogen production via steam reforming of methane with simultaneous CO_2 capture over CaO-$Ca_{12}Al_{14}O_{33}$. Energy Fuels 2010;24:2589-95.

576 [25] Dewoolkar KD, Vaidya PD. Improved hydrogen production by sorption-enhanced
577 steam methane reforming over hydrotalcite- and calcium-based hybrid materials.
578 Energy Fuels 2015;29:3870-78.
579 [26] Soltani R, Rosen MA, Dincer I. Assessment of CO_2 capture options from various
580 points in steam methane reforming for hydrogen production. Int J Hydrogen Energy
581 2014;39:20266-75.
582 [27] Angeli SD, Monteleone G, Giaconia A, Lemonidou AA. State-of-the-art catalysts
583 for CH_4 steam reforming at low temperatures. Int J Hydrogen Energy 2014;39:1979-97.
584 [28] García-Lario AL, Aznar M, Grasa GS, García T, Murillo R~~,~~. Study of nickel
585 catalysts for hydrogen production in sorption enhanced reforming process. J Power
586 Sources 2013;242:371-79.
587 [29] García-Lario AL, Aznar M, Grasa GS, Murillo R. Evaluation of process variables
588 on the performance of Sorption Enhanced Methane Reforming. J Power Sources
589 2015;285:90-99.
590 [30] Feng HZ, Lan P.Q, Wu S.F. A study on the stability of a NiO-CaO/Al_2O_3 complex
591 catalyst by La_2O_3 modification for hydrogen production, Int. J. Hydrogen Energy
592 2012;37:14161-66.
593 [31] Grasa G, Navarro MV, López JM, Díez-Martín L, Fernández JR, Murillo R.
594 Validation of the H_2 production stage via SER under relevant conditions for the Ca/Cu
595 reforming process practical application. Chem Eng J 2017;324:266-78.
596 [32] Navarro MV, López JM, García T, Grasa G, Murillo R. Catalyst evaluation for
597 high-purity H2 production by sorption-enhanced steam-methane reforming coupled to a
598 Ca/Cu process. J Power Sources 2017;363:117-25.
599 [33] Abbas SZ, Dupont V, Mahmud T. Kinetics study ~~n~~and modelling of steam
600 methane reforming process over a NiO/Al2O3 catalyst in an adiabatic packed bed. Int J
601 Hydrogen Energy 2017;42:2889-903.
602 [34] Wang F, Qi B, Wang G, Li L. Methane steam reforming: Kinetics and modelling
603 over coating catalyst in micro-channel reactor, Int. J. Hydrogen Energy 2013;38:5693-
604 704.
605 [35] Xu J, Froment GF~~,~~. Methane Steam Reforming, Methanation and Water-Gas Shift:
606 1. Intrinsic Kinetics. AIChE J 1989;35:88-96.
607 [36] Numaguchi T, Kikuchi K~~,~~. Deactivation of Bimodal Nickel Catalyst for Steam
608 Methane Reforming Reaction. Chem Eng Sci 1988;43:2295-301.

609 [37] Hou K, Hughes R. The kinetics of methane steam reforming over a Ni/a-Al_2O
610 catalyst. Chem Eng J 2001;82:311-28.
611 [38] Wei J, Iglesia E. Structural requirements and reaction pathways in methane
612 activation and chemical conversion catalyzed by rhodium. J Catal 2004;225:116-27.
613 [39] Soliman MA, Adris MA, Al-Ubaid AS, El-Nashaie SSEH. Intrinsic kinetics of
614 nickel/calcium aluminate catalyst for methane steam reforming. J Chem Tech
615 Biotechnol 1992;55:131-38.
616 [40] Ligthart DAJM, Pieterse JAZ, Hensen EJM. The role of promoters for Ni catalysts
617 in low temperature (membrane) steam methane reforming. Appl Catal A: Gen
618 2011;405:108–19.
619 [41] Rostrup-Nielsen JR, Bak Hansen JH. CO_2-Reforming of methane over transition
620 metals. J Catal 1993;144:38–49.
621 [42] Medrano JA, Hamers HP, Williams G, van Sint Annaland M, Galluci F.
622 NiO/$CaAl_2O_4$ as active oxygen carrier for low temperature chemical looping
623 applications. Appl Energy 2015;158:86-96.
624 [43] García-Lario AL, Aznar M, Martinez I, Grasa GS, García T, Murillo R.
625 Experimental study of the application of a NiO/$NiAl_2O_4$ catalyst and a CaO-based
626 synthetic sorbent on the Sorption Enhance Reforming process. Int J Hydrogen Energy
627 2015;40:219-32.
628 [44] Manovic V, Anthony EJ. Long-term behaviour of CaO-based pellets supported by
629 calcium aluminate cements in a long series of CO_2 capture cycles. Ind Eng Chem Res
630 48 (2009) 8906-8912.
631